Journal of Photochemistry and Photobiology A: Chemistry 221 (2011) 244–249

Contents lists available at ScienceDirect

Journal of Photochemistry and Photobiology A: Chemistry

journal homepage: www.elsevier.com/locate/jphotochem

Surface-plasmon-enhanced photocurrent generation of CdTe nanoparticle/titania nanosheet composite layers on Au particulate films

Tatsuya Kameyama[a], Yumi Ohno[a], Ken-ichi Okazaki[a], Taro Uematsu[b], Susumu Kuwabata[b,c], Tsukasa Torimoto[a,c,*]

[a] Department of Crystalline Materials Science, Graduate School of Engineering, Nagoya University, Chikusa-ku, Nagoya 464-8603, Japan
[b] Department of Applied Chemistry, Graduate School of Engineering, Osaka University, Suita, Osaka 565-0871, Japan
[c] Japan Science and Technology Agency, CREST, Kawaguchi, Saitama 332-0012, Japan

ARTICLE INFO

Article history:
Available online 5 March 2011

Keywords:
Semiconductor nanoparticles
Surface plasmon resonance
Photocurrent
Light energy conversion
Sensitized solar cell

ABSTRACT

Multilayer films composed of Au particle/titania nanosheet (TNS)/CdTe nanoparticle were successfully prepared using a layer-by-layer-deposition technique. CdTe nanoparticles were accumulated as the topmost layer on TNS/poly(diallyldimethylammonium) (PDDA) bilayers deposited on the substrates of an Au particle film or an F-doped SnO_2 (FTO) electrode. CdTe nanoparticles were acted as a photosensitizer. The photogenerated electrons in CdTe nanoparticles were injected into the conduction band of titania nanosheets to produce anodic photocurrent at a more positive potential than −0.4 V vs. Ag/AgCl. The magnitude of photocurrent was much larger for the films prepared on the Au particle film rather than that on the FTO electrode. Furthermore, with an increase in the thickness of (TNS/PDDA) bilayers, that is, the distance between Au and CdTe nanoparticles, the photocurrent was drastically decreased. The enhancement factor of photocurrent, defined as the ratio of the magnitude of photocurrent obtained with CdTe particle layer immobilized on Au layer to that on FTO, was varied from 2 to 10 by changing the wavelength of irradiation light. The broad peak at 520 nm appeared in the action spectrum of the enhancement factor and its profile roughly corresponded to the localized surface plasmon resonance peak of Au particle layer whose peak wavelength was ca. 540 nm. These facts indicated that the photoexcitation of the surface plasmon of Au particles, which produced a locally enhanced electric field near Au particle layer, played an important role in the increase in the photoexcitation probability of CdTe nanoparticles deposited as the topmost layer.

1. Introduction

Semiconductor nanoparticles have attracted much interest for constructing the highly efficient solar light energy conversion systems [1,2]. Since the optical properties and electronic energy structure can be adjusted depending on the particle size, size-quantized semiconductor nanoparticles are suitable materials for light absorbers or sensitizers. Recently, the sensitization of a metal oxide semiconductor having a wide band gap with narrow-band-gap semiconductor nanoparticles has been intensively investigated for developing highly efficient solar cells [3–7]. However, despite intense research efforts, the reported efficiency of the light-to-electricity energy conversion has been still small (ca. 1–4%) [4,6,7]. One promising strategy to improve the energy conversion efficiency seems to increase the amount of the incident photons adsorbed by semiconductor nanoparticles.

Recently, nanoparticles of Au and Ag having a localized surface plasmon resonance (LSPR) peak have been a promising material to improve the photochemical properties of the chromophores such as organic dyes and semiconductor nanoparticles. A locally enhanced electric field, produced in the proximity of metal nanoparticles by photoexcitation of the LSPR peak, enhanced the excitation probability of chromophores near metal particles. So far, it has been reported that the photoluminescence intensity of semiconductor nanoparticles or organic dyes in the proximity of metal particles was greatly enhanced by the photoexcitation of LSPR peak of metal particles [8–16]. The irradiation to dye molecules immobilized near Au nanoparticles produced much larger photocurrent than those without Au particles [17,18]. Furthermore, very recently, Hupp and co-workers reported that ruthenium dyes adsorbed on amorphous TiO_2 layer, which were prepared on the substrate of an Ag particle-immobilized F-doped SnO_2 electrode, effectively generated the photocurrent by photoexciting LSPR peak of Ag particle layer as the bottom layer [19]. Therefore, if metal

* Corresponding author at: Department of Crystalline Materials Science, Graduate School of Engineering, Nagoya University, Chikusa-ku, Nagoya 464-8603, Japan. Tel.: +81 52 789 4614; fax: +81 52 789 5299.
E-mail address: torimoto@apchem.nagoya-u.ac.jp (T. Torimoto).

1010-6030/$ – see front matter © 2011 Elsevier B.V. All rights reserved.
doi:10.1016/j.jphotochem.2011.02.029

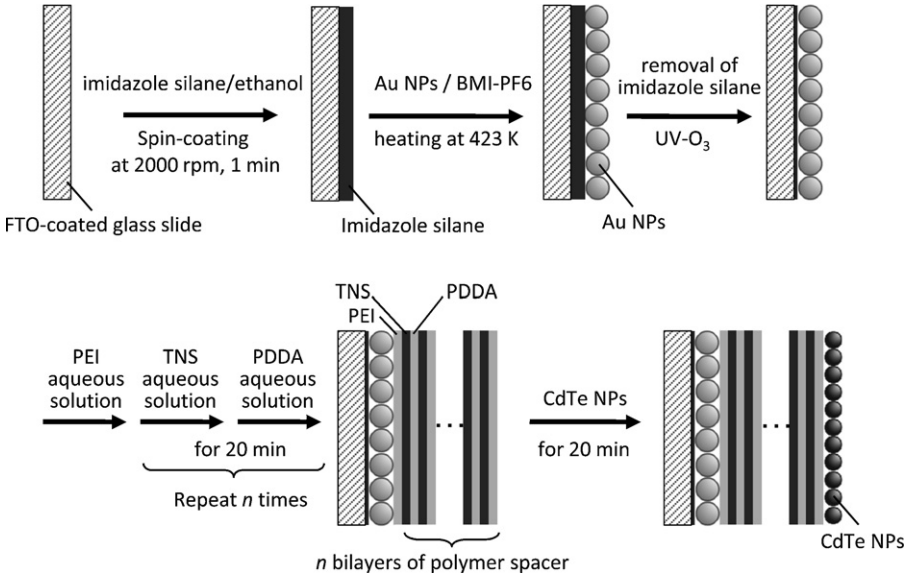

Fig. 1. Schematic illustration of preparation procedure of Au/(TNS/PDDA)$_n$/CdTe multilayer films.

nanoparticles is appropriately incorporated in the photoelectrodes of semiconductor nanoparticle-metal oxide nanocomposite films, the light-to-electricity conversion efficiency is expected to be increased due to the enhancement of photoexcitation probability of semiconductor nanoparticles by an LSPR-induced electric field, but this has not been attempted.

In this study, we prepared the multilayer films of Au particle/titania nanosheet/CdTe nanoparticle using a layer-by-layer-deposition technique and investigated their photoelectrochemical properties. The irradiation to the films produced the anodic photocurrent, the magnitude of which was enhanced with the presence of Au particle layer as the bottom layer but decreased with an increase in the distance between Au and CdTe nanoparticles. The results could be explained by the modulation of photoexcitation probability of the topmost CdTe nanoparticle layer by a locally enhanced electric field near the Au particle layer as the bottom layer.

2. Experimental

2.1. Materials

An IL of 1-butyl-3-methylimidazolium hexafluorophosphate (BMI-PF6) was purchased from Kanto Chemical Co. Inc. Polyethyleneimine (PEI) was purchased from Tokyo Chemical Industry, and chemicals of poly(diallyldimethylammonium) (PDDA) chloride, and tellurium powder were obtained from Aldrich. A silane coupling agent of 3′-(trimethoxysilyl)propoxy-3-hydroxypropyl-1,3-diazole (Si-imidazole) was kindly provided by Nippon Mining & Metals Co. Ltd. Other reagents were supplied by Kishida Reagents Chemicals. A colloidal suspension of titania nanosheet was prepared via the chemical exfoliation of a protonic titanate with the lepidocrocite-type layered structure $H_{0.7}Ti_{1.825}\square_{0.175}O_4{\cdot}H_2O$, where □ is vacancy of the crystal, with use of tetrabutylammonium hydroxide [20,21]. Thioglycolic acid (TGA)-modified CdTe nanoparticles having negative surface charges were synthesized by previously reported methods [22,23]. The size of CdTe nanoparticles were estimated to 4.0 nm by the reported relation between the energy gap and the particle size [22]. Aqueous solutions were prepared with purified water just before use by a Millipore Milli-Q system.

2.2. Fabrication of multilayer thin films consisting of Au/TNS/CdTe layers

Multilayer films were fabricated using the electrostatic layer-by-layer deposition technique, by which an Au layer was separated from CdTe layer with a titania nanosheet/polymer spacer layer having various thicknesses. Au nanoparticles were immobilized on F-doped SnO_2 (FTO)-coated glass substrate or quartz substrate using previously reported methods [16]. Au nanoparticles with the average size of 2.6 nm were prepared in BMI-PF6 by the sputter deposition of gold [16,24,25]. A 60 mm^3 aliquot of the thus-obtained IL solution containing Au nanoparticles ([Au] = 5.9 mmol dm^{-3}) was spread on the substrate modified with Si-imidazole as a cross linker and then heat-treated at 423 K under vacuum. After washing the IL with acetonitrile, thus-obtained Au nanoparticle-immobilized FTO substrate was kept in a UV/ozone treatment chamber for 14 h to remove the organic Si-imidazole cross-linker layer under Au particle films and then used for the layer-by-layer deposition of TNS thin films.

The preparation procedure of multilayer films was schematically illustrated in Fig. 1. Au nanoparticle-immobilized substrate was first immersed in an aqueous solution containing 2.5 g dm^{-3} PEI (pH 9.0) for 20 min to introduce positive charges onto the surface. The resulting substrate was alternately dipped in a aqueous solution containing 0.08 g dm^{-3} TNS (pH 9.0) and an aqueous solution containing 5.0 g dm^{-3} PDDA (pH 9.0) for 20 min each according to previous reported method [21]. After each deposition, the substrate was washed with water and dried in nitrogen gas flow. A series of these operations was repeated n times to obtain a spacer layer of (TNS/PDDA)$_n$ on Au particle layer (Au/(TNS/PDDA)$_n$). Finally, CdTe nanoparticles were layer-by-layer-accumulated as the topmost layer by immersing an aqueous solution containing TGA-modified CdTe nanoparticles (2.9×10^{15} particles dm^{-3}) for 1 h, followed by washing with water and drying. The thus-obtained multilayer film was denoted as Au/(TNS/PDDA)$_n$/CdTe. For comparison, multilayer films without an Au layer, denoted as FTO/(TNS/PDDA)$_n$/CdTe, were prepared in the same way except for the use of bare FTO glass instead of Au-immobilized substrates.

2.3. Characterizations

The size of Au nanoparticles was determined by using a transmission electron microscope (TEM) (Hitachi, H7650) with

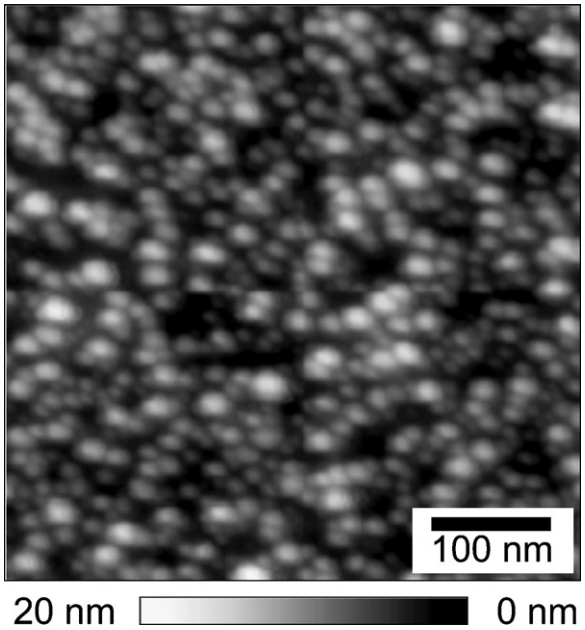

Fig. 2. A typical AFM image of Au nanoparticle layer deposited on quartz substrate-modified with Si-imidazole. The immobilization was conducted by the heat treatment at 423 K.

an acceleration voltage at 100 kV. UV–visible absorption spectra were measured using a spectrophotometer (Agilent Technology 8453A). Photoelectrochemical properties of the films were measured in an acetonitrile solution containing 0.10 mol dm^{-3} $LiClO_4$ and 0.10 mol dm^{-3} triethanolamine (TEOA) as a sacrificial electron donor. The potential was determined against an Ag/AgCl (3 mol dm^{-3} NaCl) reference electrode and a Pt wire was used as a counter electrode. Photocurrents were measured under a nitrogen atmosphere using the lock-in technique; the photocurrent was detected with a potentiostat (Hokuto Denko, HA-151) and amplified with a lock-in amplifier (NF circuit, LI5640) by extracting the signal that was synchronized with irradiation. Light irradiation was performed by chopping at 7 Hz a light ($\lambda > 350$ nm) that was obtained by passing light from a 300 W Xe lamp (EAGLE, X300) through a UV cut-off filter. The irradiation intensity at the electrode surface was 0.17 W cm^{-2}. Action spectra of photocurrents were obtained with monochromatic light irradiation using a monochromator (JASCO, CT-10T) equipped with a Xe lamp. The incident photon-to-current efficiency (IPCE) was calculated by dividing the number of electrons detected in the photocurrents by that of incident photons.

3. Results and discussion

3.1. Layer-by-layer-deposition of Au/(TNS/PDDA)$_n$/CdTe multilayer films

Fig. 2 shows a typical AFM image of Au nanoparticle layer deposited on a quartz glass substrate modified with Si-imidazole before the UV/ozone treatment. Au nanoparticles were densely immobilized on the substrate surface to form a uniform particle layer without large aggregates, due to the adsorption of imidazole group of Si-imidazole to Au nanoparticles as we reported before [16]. The size distribution of immobilized particles was estimated by measuring the vertical height of each particle. The average size of Au particles immobilized was determined to 9.1 nm with the standard deviation of 1.9 nm. Since Au nanoparticles as-sputter-deposited in BMI-PF6 had the average diameter of 2.6 nm, the immobilization of these Au particles with heat treatment at 423 K caused not only dense accumulation of particles but also coalescence between the particles to form larger ones.

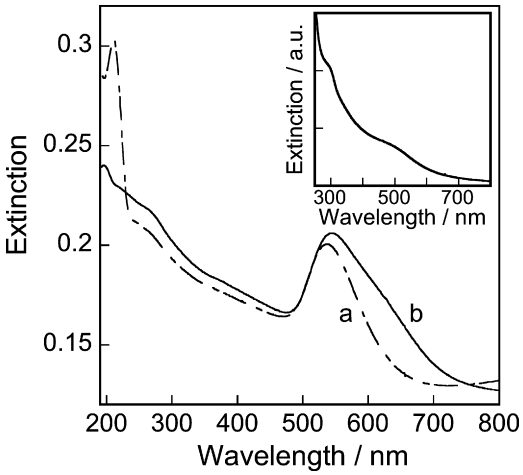

Fig. 3. Changes in the extinction spectra of Au-particle-deposited quartz substrate before (a) and after UV/ozone treatment (b). (inset) Extinction spectrum of Au nanoparticles sputter-deposited in BMI-PF6.

Fig. 3 shows the extinction spectra of Au nanoparticle-immobilized quartz substrates before and after the UV/ozone treatment. Au particle films deposited on Si-imidazole-modified substrate exhibited a broad peak around 535 nm assigned to the LSPR peak of Au nanoparticles, accompanied with an absorption peak at 220 nm originating from Si-imidazole cross-linker layer. It should be noted that the immobilization of Au particles developed relatively sharp LSPR peak, though Au nanoparticles sputter-deposited in BMI-PF6 exhibited a broader shoulder at 520 nm assigned to the LSPR peak (the inset of Fig. 2). Since it is well known that the LSPR peak becomes remarkably sharp with an increase in the size of spherical Au particles from 2 to 8 nm [26], the observed optical changes originated from the increase in the size of Au particles during the immobilization, as supported by AFM measurement (Fig. 2).

As mentioned below, the Si-imidazole layer attached on FTO substrates was an insulating layer and blocked the electron transfer between Au particles and FTO electrodes. Therefore, we removed this organic layer from as-deposited films by the UV/ozone treatment. As shown in the spectrum (b) of Fig. 3, the absorption peak assigned to Si-imidazole layers at 220 nm disappeared in the absorption spectrum of the Au particle films with the UV/ozone treatment. On the other hand, the LSPR peak of the Au particles immobilized on substrates was broadened with the slight red shift of the peak wavelength from 535 to 540 nm. Although the remarkable changes in the surface morphology of the Au particle layer on quartz substrate was not observed by AFM measurement (not shown), the observed broadening of LSPR peak indicated that the size of Au particles was slightly increased due to the partial coalescence between particles during the removal of Si-imidazole layer with UV/ozone treatment. In the following photoelectrochemical experiments, the Au particle-immobilized FTO electrode obtained with UV/ozone treatment was used for the substrates.

Layer-by-layer deposition is a useful strategy to prepare multilayer films having a desired stacked structure, because precise control of the distance between metal films and semiconductor nanoparticles is a prerequisite for the fine tuning of photoelectrochemical properties of the resulting films. Composite layers of TNS/PDDA were deposited on the surface of Au nanoparticle films as a spacer layer before the immobilization of CdTe nanoparticles, as illustrated in Fig. 1. Fig. 4 shows changes in the absorption spectra of Au/(TNS/PDDA)$_n$ films with accumulation of TNS/PDDA bilayers.

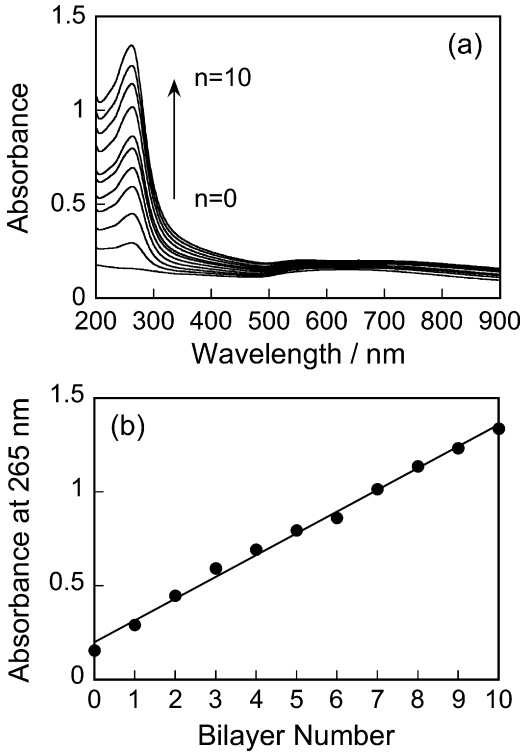

Fig. 4. (a) Absorption spectra of Au/(TNS/PDDA)$_n$ films depending on the number of the accumulation. (b) Changes in the absorbance at 265 nm with the number of the accumulation.

The absorption peak assigned to titania nanosheets was observed at 265 nm, whose intensity was linearly increased with an increase in the accumulation number of bilayers, *n*. These results indicated that a constant amount of spacer layer was accumulated in each deposition cycle of the TNS/PDDA bilayer. By comparing the slope of increment in absorbance at 265 nm (ca. 0.12 per bilayer) to the previously reported absorbance changes per TNS layer (0.127 per TNS layer) observed for TNS multilayer films [27], it was suggested that a TNS monolayer could be immobilized per deposition cycle. The thickness of TNS/PDDA bilayer was determined by razor-blade scratching and subsequent imaging with AFM. The linear relation was observed between the depth of scratch marks in the film and the accumulation number of TNS/PDDA bilayers. From the slope of the linear relation, it was found that the increment in the film thickness per (TNS/PDDA) bilayer was ca. 2.6 nm.

The anionic surface charges of TGA-modified CdTe particles enabled the accumulation of a CdTe particle monolayer on the topmost positively charged PDDA on (TNS/PDDA)$_n$ layer through electrostatic interaction. The resulting nanocomposite films with or without an Au particle layer as the bottom layer exhibited the sharp band gap photoluminescence with peak wavelength at 680 nm (not shown), which agreed with that of CdTe nanoparticle dispersed in an aqueous solution. The fact indicated that CdTe particles were successfully deposited on the (TNS/PDDA)$_n$ layers to form multilayer films of Au/(TNS/PDDA)$_3$/CdTe or FTO/(TNS/PDDA)$_3$/CdTe.

3.2. Photoelectrochemical properties of multilayer films

Fig. 5 shows the photocurrent–potential curves of Au/(TNS/PDDA)$_3$/CdTe and FTO/(TNS/PDDA)$_3$/CdTe films. It should be noted that the much smaller photocurrent was observed for the films using Au nanoparticles substrates without UV/ozone treatment (not shown). These facts suggested that the organic layer of Si-imidazole on FTO, used as a cross-linker layer to immobilize Au

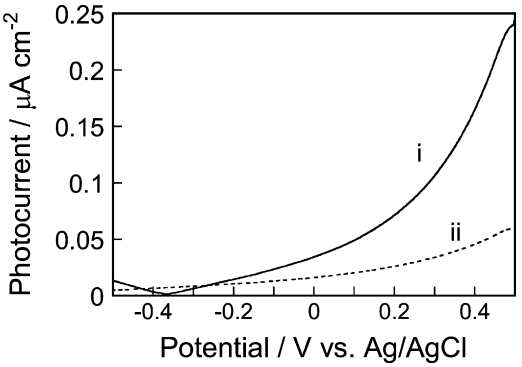

Fig. 5. Photocurrent–potential curves of multilayer films with Xe lamp irradiation (λ > 350 nm). The films used were Au/(TNS/PDDA)$_3$/CdTe (i) and FTO/(TNS/PDDA)$_3$/CdTe (ii).

particles, was an insulating layer and then the UV/ozone treatment oxidatively removed the Si-imidazole layer to enable the electron transfer from TNS layers to FTO substrate via Au particle layer. As shown in Fig. 5, the anodic photocurrents were observed at more positive potential than −0.4 V vs. Ag/AgCl in both cases, indicating that the prepared nanocomposite films exhibited the behavior similar to n-type semiconductor photoelectrodes, regardless of the presence of Au nanoparticle layer as the bottom layer. On the other hand, the magnitude of photocurrent obtained became larger for the film with use of Au nanoparticle-immobilized substrate than that deposited on FTO substrate only.

Fig. 6b and c shows the action spectra of photocurrent obtained by FTO/(TNS/PDDA)$_3$/CdTe and Au/(TNS/PDDA)$_3$/CdTe films, respectively, under the potential application at 0.5 V vs. Ag/AgCl. The photocurrent was observed by the monochromatic light irradiation with wavelength shorter than ca. 700 nm and their magnitude was enlarged with a decrease in the wavelength of irradiation light. The onset wavelength of photocurrent generation was in good agreement with the absorption onset of CdTe nanoparticles used, 700 nm (Fig. 6a). These facts indicated that the photocurrents resulted from photoexcitation of the CdTe nanoparticles immobilized onto the films as the topmost layer and also that no coalescence of CdTe nanoparticles occurred during the immobilization. As schematically shown in the inset of Fig. 6c, CdTe nanoparticles were acted as a photosensitizer and then the photogenerated electrons in CdTe nanoparticles were injected into the conduction band of titania nanosheets, followed by the transfer from titania nanosheets through the PDDA layer by the electron tunneling process to the Au particle-immobilized FTO electrode, resulting in the generation of anodic photocurrents. Furthermore the higher IPCE value was obtained at each wavelength of irradiation light for the films deposited on Au-nanoparticle layers than that of the films without Au particles. Since the amount of CdTe nanoparticles deposited assumed to be constant regardless of the (TNS/PDDA)$_n$ spacer layer, being similar to our previous paper [16], the observed changes in the photocurrent intensity resulted from the presence of an Au particle layer at the bottom of the multilayer films.

In the cases of rutile or anatase TiO_2 photoelectrode modified with Au particles [27–29], recently, it has been reported that the photoexcitation of LSPR peaks induced the direct electron transfer from Au particles to the conduction band of TiO_2, in which the action spectra of photocurrent agreed well with the shape of LSPR peak of Au particles. This was not true of the present case, because the direction of electron flow observed in the present study was opposite to those previously reported for crystalline TiO_2 modified with Au, that is, the photogenerated electrons in the CdTe particles could be injected into titania nanosheet layers and then moved

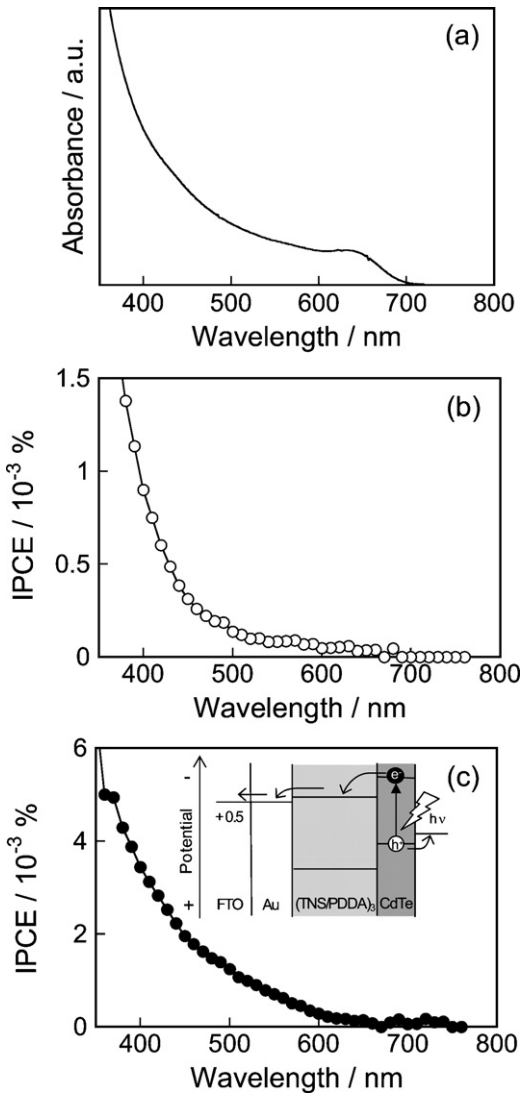

Fig. 6. (a) Absorption spectrum of CdTe nanoparticles dispersed in an aqueous solution. (b and c) Action spectra of the photocurrent at the potential application of 0.5 V vs. Ag/AgCl. The electrodes used were FTO/$(TNS/PDDA)_3$/CdTe (b) and Au/$(TNS/PDDA)_3$/CdTe films (c).

from titania nanosheets to FTO electrode via Au particles to produce anodic photocurrents as shown in Figs. 5 and 6c, and also because the peak corresponding to LSPR peak of Au was not observed in the action spectra of photocurrent for Au/$(TNS/PDDA)_3$/CdTe (Fig. 6c). Therefore, we concluded that the anodic photocurrent observed in the present study was generated by the photoexcitation of CdTe particles, and then the contribution of the direct electron transfer from the photoexcited Au particles to titania nanosheet to the photocurrent were negligibly small, if any.

It has been reported that a locally enhanced electric field is produced in the proximity of Au nanoparticles by photoexcitation of the LSPR peak and enlarges the photoexcitation probability of semiconductor nanoparticles located in the vicinity of Au particles, resulting in the enhancement of photoluminecence (PL) of semiconductor nanoparticles [8,11–13,15,16]. Furthermore the degree of PL enhancement has been reported to be greatly dependent on the wavelength of irradiation [12,13]. Therefore, it is interesting to investigate the relationship between the degree of photocurrent enhancement and wavelength of irradiation light. Fig. 7 shows the wavelength-dependence of enhancement factor of photocurrent, I_{Au}/I_{FTO}, which was defined as the ratio of the magnitude

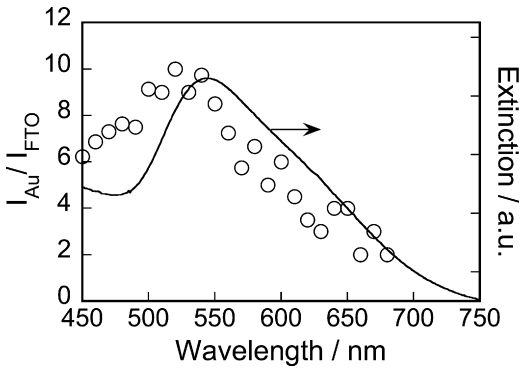

Fig. 7. Wavelength-dependence of the photocurrent enhancement factor (open circles). The extinction spectrum of the Au particle layer used is also shown (solid line).

of photocurrent obtained with Au/$(TNS/PDDA)_3$/CdTe to that with FTO/$(TNS/PDDA)_3$/CdTe. The enhancement factor of I_{Au}/I_{FTO} was varied from 2 to 10 at by changing the wavelength of irradiation light. These obtained values were comparable to those previously reported for photoluminescence enhancement of semiconductor nanoparticles, 3–10 [11,13,14]. The broad peak with wavelength at 520 nm was observed in the wavelength dependence of I_{Au}/I_{FTO} and then its peak profile roughly corresponded to the LSPR peak of Au particle films whose peak wavelength was ca. 540 nm.These facts indicated that the photoexcitation of the surface plasmon of Au particles, which produced a locally enhanced electric field near Au particle layer, played an important role in the increase in the photoexcitation probability of CdTe nanoparticles. We should note that there is a little deviation between enhancement factor and extinction spectrum of Au particle films. It may be caused by the differences in the contribution for the photocurrent enhancement among a variety of size of Au particles. In the present study, smaller Au particles, which shows LSPR peak at shorter wavelength than that of larger one, have seemed to work more efficiently.

The magnitude of photocurrent was greatly dependent on the thickness of spacer layer, $(TNS/PDDA)_n$. Fig. 8 shows the IPCE at 540 nm of Au/$(TNS/PDDA)_n$/CdTe films as a function of the number of bilayers, n. The IPCE value increased by introducing 3 layers of spacer between Au and CdTe films, and then rapidly decreased

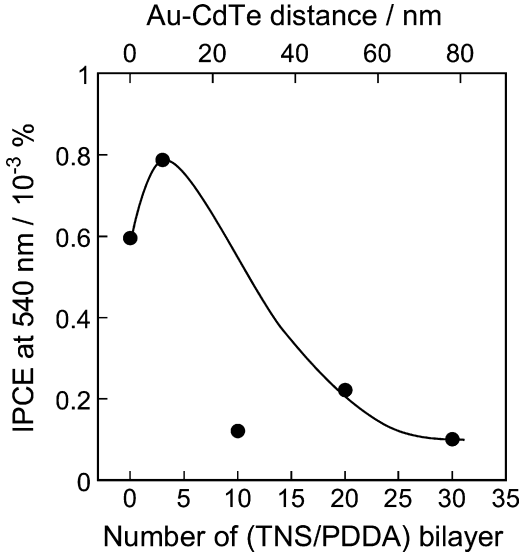

Fig. 8. Relationship between IPCE at 540 nm of Au/$(TNS/PDDA)_n$/CdTe films as a function of the number of bilayers, n.

with an increase in the number of $(TNS/PSSA)_n$ layer beyond $n = 3$, though the decrease tendency of $n = 10$ is slightly differed from the others, probably due to an experimental error. As mentioned above, the distance between Au particles and CdTe particles ($d_{Au-CdTe}$) increased with an increase in the bilayer number of $(TNS/PDDA)_n$, in which the increment in the film thickness per (TNS/PDDA)bilayer was ca. 2.6 nm. The results in Fig. 8 indicated that the enhancement of photocurrent generation of CdTe particles by the Au particle layer became remarkable at $d_{Au-CdTe}$ of 7.8 nm but CdTe particles with $d_{Au-CdTe}$ beyond 26 nm could not be effectively photoexcited by the LSPR-induced electric field of Au particles. Similar distance-dependence has been reported for the photoluminescence enhancement of semiconductor nanoparticles immobilized in the proximity of Au films [8,11]. These phenomena were explained by the energetic interaction between metal and semiconductor nanoparticles. It is well known that the photoexcitation of LSPR peaks of Au nanoparticles produces a locally enhanced electric field, which can increase the probabilities of photoexcitation of semiconductor nanoparticles, but the intensity of LSPR-induced electric field drastically decays with a distance from the metal surface. Considering these facts, the decrease in IPCE with the films having the $(TNS/PDDA)_n$ bilayer number larger than $n = 3$, shown in Fig. 8, could be explained by the decrease in the photoexcitation probability of CdTe nanoparticles; that is, with an increase in $d_{Au-CdTe}$ more than 7.8 nm, the number of CdTe particles photoexcited by LSPR-induced electric field was greatly diminished. It should be noted that the Au/$(TNS/PDDA)_n$/CdTe film with $n = 30$ exhibited almost the same IPCE at 540 nm as that for the film ($n = 3$)without Au particles(ca. 1×10^{-4}%) in Fig. 6b, suggesting that the intensity of the LSPR-induced electric field became too small at the outer surface of the $(TNS/PDDA)_{30}$ spacer layer to effectively photoexcite CdTe particles deposited on it, due to the large distance of $d_{Au-CdTe}$, ca. 80 nm.On the other hand, the IPCE obtained for the film with $n = 0$, that is, without TNS/PDDA spacer layer, became smaller than that obtained with the spacer thickness of $n = 3$. Since the probability of energy transfer from CdTe to Au was remarkably enhanced with a decrease in $d_{Au-CdTe}$, the observed slight decrease in IPCE at $n = 0$ was due to the quenching of the photoexcited CdTe with the energy transfer to Au particle film, resulting in the optimum value of IPCE at $n = 3$.

4. Conclusion

We have successfully accumulated CdTe nanoparticles on TNS/PDDA bilayers. Photoexcitation of CdTe nanoparticles generated anodic photocurrent. The magnitude of photocurrent was enhanced with the presence of Au particle layer as the bottom layer but decreased with an increase in the spacer thickness of TNS/PDDA bilayers, probably because photoexcitation probability of CdTe nanoparticles was modulated by the locally enhanced electric field formed with the photoexcitation of LSPR peak of Au particles, the degree being dependent on the distance between CdTe and Au particles. Although the Au particles films exhibiting the LSPR peak around 540 nm was only used in this paper, the film of larger Au particles or Au rods having the LSPR band in the longer-wavelength region (~1000 nm) enables the effective enhancement of photocurrent generation with the irradiation of the near-infrared light, resulting in the improvement of the energy conversion efficiency of semiconductor nanoparticle-sensitized solar cells. Work in this direction is in progress.

Acknowledgments

This work was supported by a Grant-in-Aid for Scientific Research (A) (No. 20245031) from the Japan Society for the Promotion of Science and by a Grant-in-Aid for Scientific Research on Priority Areas "Strong Photon-Molecule Coupling Fields (No. 470)" (No. 19049009) from the Ministry of Education, Culture, Sports, Science and Technology of Japan. One of the authors (T.K.) expresses his gratitude to a Grant-in-Aid for JSPS Fellows.

References

[1] P.V. Kamat, K. Tvrdy, D.R. Baker, J.G. Radich, Chem. Rev. 110 (2010) 6664.
[2] A.J. Nozik, M.C. Beard, J.M. Luther, M. Law, R.J. Ellingson, J.C. Johnson, Chem. Rev. 110 (2010) 6873.
[3] R. Vogel, P. Hoyer, H. Weller, J. Phys. Chem. 98 (1994) 3183.
[4] H. Lee, H.C. Leventis, S.J. Moon, P. Chen, S. Ito, S.A. Haque, T. Torres, F. Nuesch, T. Geiger, S.M. Zakeeruddin, M. Gratzel, M.K. Nazeeruddin, Adv. Func. Mater. 19 (2009) 2735.
[5] T. Sasamura, K. Okazaki, R. Tsunoda, A. Kudo, S. Kuwabata, T. Torimoto, Chem. Lett. 39 (2010) 619.
[6] S.Q. Huang, Q.X. Zhang, X.M. Huang, X.Z. Guo, M.H. Deng, D.M. Li, Y.H. Luo, Q. Shen, T. Toyoda, Q.B. Meng, Nanotechnology 21 (2010) 375201.
[7] V. Gonzalez-Pedro, X. Xu, I. Mora-Sero, J. Bisquert, ACS Nano 4 (2010) 5783.
[8] O. Kulakovich, N. Strekal, A. Yaroshevich, S. Maskevich, S. Gaponenko, I. Nabiev, U. Woggon, M. Artemyev, Nano Lett. 2 (2002) 1449.
[9] K. Aslan, I. Gryczynski, J. Malicka, E. Matveeva, J.R. Lakowicz, C.D. Geddes, Curr. Opin. Biotechnol. 16 (2005) 55.
[10] J.R. Lakowicz, Plasmonics 1 (2006) 5.
[11] V.K. Komarala, Y.P. Rakovich, A.L. Bradley, S.J. Byrne, Y.K. Gun'ko, N. Gaponik, A. Eychmuller, Appl. Phys. Lett. 89 (2006) 253118.
[12] Y. Ito, K. Matsuda, Y. Kanemitsu, Phys. Rev. B 75 (2007) 033309.
[13] K. Matsuda, Y. Ito, Y. Kanemitsu, Appl. Phys. Lett. 92 (2008) 211911.
[14] Y. Chen, K. Munechika, I.J.L. Plante, A.M. Munro, S.E. Skrabalak, Y. Xia, D.S. Ginger, Appl. Phys. Lett. 93 (2008) 053106.
[15] W.W. Zhong, Anal. Bioanal. Chem. 394 (2009) 47.
[16] T. Kameyama, Y. Ohno, T. Kurimoto, K. Okazaki, T. Uematsu, S. Kuwabata, T. Torimoto, Phys. Chem. Chem. Phys. 12 (2010) 1804.
[17] T. Arakawa, T. Munaoka, T. Akiyama, S. Yamada, J. Phys. Chem. C 113 (2009) 11830.
[18] T. Akiyama, K. Aiba, K. Hoashi, M. Wang, K. Sugawa, S. Yamada, Chem. Commun. 46 (2010) 306.
[19] S.D. Standridge, G.C. Schatz, J.T. Hupp, J. Am. Chem. Soc. 131 (2009) 8407.
[20] T. Sasaki, M. Watanabe, J. Am. Chem. Soc. 120 (1998) 4682.
[21] T. Sasaki, Y. Ebina, T. Tanaka, M. Harada, M. Watanabe, G. Decher, Chem. Mater. 13 (2001) 4661.
[22] A.L. Rogach, T. Franzl, T.A. Klar, J. Feldmann, N. Gaponik, V. Lesnyak, A. Shavel, A. Eychmuller, Y.P. Rakovich, J.F. Donegan, J. Phys. Chem. C 111 (2007) 14628.
[23] T. Uematsu, H. Kitajima, T. Kohma, T. Torimoto, Y. Tachibana, S. Kuwabata, Nanotechnology 20 (2009) 215302.
[24] T. Torimoto, K. Okazaki, T. Kiyama, K. Hirahara, N. Tanaka, S. Kuwabata, Appl. Phys. Lett. 89 (2006) 243117.
[25] K.I. Okazaki, T. Kiyama, K. Hirahara, N. Tanaka, S. Kuwabata, T. Torimoto, Chem. Commun. (2008) 691.
[26] J.H. Hodak, A. Henglein, G.V. Hartland, J. Chem. Phys. 112 (2000) 5942.
[27] N. Sakai, T. Sasaki, K. Matsubara, T. Tatsuma, J. Mater. Chem. 20 (2010) 4371.
[28] Y. Tian, T. Tatsuma, J. Am. Chem. Soc. 127 (2005) 7632.
[29] Y. Nishijima, K. Ueno, Y. Yokota, K. Murakoshi, H. Misawa, J. Phys. Chem. Lett. 1 (2010) 2031.